

# Distance Form Factor of a Homogeneous Poisson Point Process and a Coulomb Gas

Matteo Massaro<sup>1</sup> and Adolfo del Campo<sup>1,2</sup>

<sup>1</sup>*Department of Physics and Materials Science, University of Luxembourg, L-1511 Luxembourg, Luxembourg*<sup>\*</sup>

<sup>2</sup>*Donostia International Physics Center, E-20018 San Sebastián, Spain*

We introduce a distance form factor (DFF) for the characterization of spatial patterns associated with point processes. Specifically, the DFF is defined in terms of the averaged even Fourier transform of the distance between any pair of points. We focus on homogeneous Poisson point processes and derive the explicit expression for the DFF in  $d$ -spatial dimensions. The DFF can then be found in terms of the even Fourier transform of the probability distribution for the distance between two independent and uniformly distributed random points on a  $d$ -dimensional ball, arising in the ball line picking problem. The relation between the DFF and the set of  $n$ -order spacing distributions is further established. The DFF is analyzed in detail for  $d = 1, 2, 3$  and in the infinite-dimensional case, as well as for the  $d$ -dimensional Coulomb gas, as an interacting point process.

## I. INTRODUCTION

A point process is a probabilistic model used to describe the random distribution of points in a given space, making it a versatile tool with wide-ranging applications across fields such as physics, engineering, computer science, finance, ecology, and epidemiology [1, 2]. Among the various types of point processes, the Poisson Point Process (PPP) stands out as the most widely studied due to its simplicity and analytical tractability.

In quantum physics, PPPs play a significant role in the analysis of quantum chaos [3, 4]. According to the Bohigas-Giannoni-Schmit conjecture, the spectral properties of quantum chaotic systems are governed by random matrix theory [5]. A key aspect of diagnosing quantum chaos involves the statistical analysis of a Hamiltonian ensemble, focusing on metrics such as eigenvalue spacings and the spectral form factor—essentially, the Fourier transform of the eigenvalue distribution [6–9]. Depending on the symmetries of the Hamiltonian, an established correspondence exists between spectral statistics and PPPs, further highlighting the significance of PPPs in the study of quantum systems [4, 10].

Another important application of point processes arises in nonequilibrium statistical mechanics, particularly in the study of phase transitions. It is well known that the occurrence of a phase transition in finite time leads to the formation of topological defects [11] according to the celebrated Kibble-Zurek mechanism [12–16]. Defect formation similarly occurs at fast quenches [17–19]. Examples of such defects include kinks in scenarios of parity-symmetry breaking [20–24] and vortices in the case of  $U(1)$  symmetry breaking, e.g., during the formation of a Bose-Einstein condensate [25–28], a strongly-coupled superconductor [29] or a superfluid [17, 19], such as a unitary superfluid Fermi gas [30, 31]. Point processes have been proposed for modeling the spatial patterns of point-like topological defects spontaneously formed across a phase transition [32, 33]. Specifically, a PPP with intensity set by the Kibble-Zurek mechanism has been shown to accurately describe the statistical features of spatial patterns of kinks and vortices. The analysis of such patterns motivates our study.

The characterization of point processes is commonly done in terms of the structure factor, defined as the Fourier transform of the two-point correlation function. Structure factors provide insights into the degree of order, randomness, or clustering in the system. In this work, we introduced the Distance Form factor (DFF) as a complementary measure to the structure factor. The DFF is defined as the averaged even Fourier transform of the distance between any pair of points. We motivate this measure in Sec. II. Section III introduces its definition and presents numerical examples for regular, quasi-periodic, and random patterns. It further establishes the dual relations between the DFF and distance distribution. The computation of the DFF for a homogeneous Poisson point process is presented in Sec. IV. Section V is devoted to the characterization of the DFF, including its asymptotics, evaluation in special cases, connection to quantum chaos, higher-order spacing distributions, and large-dimensional limit. We close with a summary and discussions in Sec. VII.

## II. MOTIVATION FOR THE DISTANCE FORM FACTOR

In the study of liquids and solids, the structure factor is a useful tool to analyze and identify different phases of matter [34]. It is defined as

$$S(\mathbf{k}) := \frac{1}{N} \left\langle \sum_{i,j=1}^N e^{i\mathbf{k} \cdot (\mathbf{r}_i - \mathbf{r}_j)} \right\rangle, \quad (1)$$

where  $\mathbf{r}_i$  denotes the position of the generic  $i$ -th constituent of the sample system, such as an atom in a gas or on a crystal lattice. Typically, the positions of the  $N$  constituents, which we generically refer to as particles, are not static but change over time. Therefore, the definition of  $S(\mathbf{k})$  involves averaging  $\langle \cdot \rangle$  over different configurations, determined by the varying particle locations measured within a finite time window, or more generally, drawn from a given ensemble. When these positions follow a periodic pattern, as in a crystal,  $S(\mathbf{k})$  exhibits prominent peaks, indicating such regularity. In contrast, the opposite scenario, typical of an ideal gas, is characterized by a complete lack of fine structure due to the absence of interactions. In this case, the system can be modeled as a spatial point process, where points are randomly, uniformly, and indepen-

<sup>\*</sup> [matteo.massaro@uni.lu](mailto:matteo.massaro@uni.lu)

dently scattered within the system domain for each configuration. We will primarily focus on two types of such stochastic processes: the binomial point process (BPP) and the homogeneous Poisson point process (PPP), for which we now briefly review their definitions.

Let us consider a bounded Borel set  $W \subset \mathbb{R}^d$  with positive measure  $|W| > 0$ , and let  $N \in \mathbb{N}$ . An  $N$ -BPP  $X$  consists of  $N$  random points  $\{X_1, \dots, X_N\}$ , which are independently and uniformly distributed over  $W$  [35]. Consequently, for any Borel set  $B \subset W$ , the probability that the number of points falling within  $B$  is  $\mathcal{N}(B) = k$  follows the binomial distribution:

$$P(\mathcal{N}(B) = k) = \binom{N}{k} \left( \frac{|B|}{|W|} \right)^k \left( 1 - \frac{|B|}{|W|} \right)^{N-k}, \quad 0 \leq k \leq N. \quad (2)$$

The PPP emerges as the limit of the BPP when the volume of the domain  $W$  is sent to infinity while keeping the point density  $\lambda = \frac{N}{|W|}$  fixed. In this limit, for a bounded Borel set  $B \subset W$ , the probability that  $k$  points fall within  $B$  converges to:

$$P(\mathcal{N}(B) = k) \rightarrow e^{-\lambda|B|} \frac{(\lambda|B|)^k}{k!}. \quad (3)$$

In general, a point process  $X$  is a homogeneous PPP on  $W$  with intensity  $\lambda$  if the following two conditions are satisfied [35]:

- The number of points  $\mathcal{N}(B)$  in a bounded Borel set  $B \subset W$  is a Poisson-distributed random variable with mean  $\lambda|B|$ .
- Given  $s$  disjoint bounded Borel sets within  $W$ , the number of points in each set forms a collection of  $s$  independent random variables.

Having reviewed the relevant definitions, we now consider a BPP consisting of  $N$  points distributed within a disk of radius  $R$  as an introductory example to demonstrate the calculation of the structure factor. In this scenario,  $S(\mathbf{k})$  can be computed from the definition (1) as

$$\begin{aligned} S_{\text{BPP}(N)}(\mathbf{k}) &= \frac{1}{N} \left( N + N(N-1) \langle e^{i\mathbf{k} \cdot (\mathbf{r}_1 - \mathbf{r}_2)} \rangle \right) \\ &= 1 + (N-1) \iint_{\text{disk}(R)} \frac{1}{(\pi R^2)^2} e^{i\mathbf{k} \cdot (\mathbf{r}_1 - \mathbf{r}_2)} d\mathbf{r}_1 d\mathbf{r}_2 \\ &= 1 + (N-1) \left( \frac{2J_1(kR)}{kR} \right)^2, \end{aligned} \quad (4)$$

where  $J_1$  is the Bessel function of the first kind, and  $k$  is the modulus of the vector  $\mathbf{k}$ .

The structure factor of a homogeneous PPP,  $S_{\text{PPP}}(\mathbf{k})$ , defined on the same disk, can be derived similarly. In fact, it simply involves averaging the  $S_{\text{BPP}(N)}(\mathbf{k})$  expression over  $N$  according to the Poisson distribution. As a result,  $S_{\text{PPP}}(\mathbf{k})$  is obtained by replacing  $N$  in Eq. (4) with the intensity  $\lambda$  of the PPP.

From the previous examples, it is clear that the structure factor is a useful tool for characterizing spatial point patterns.

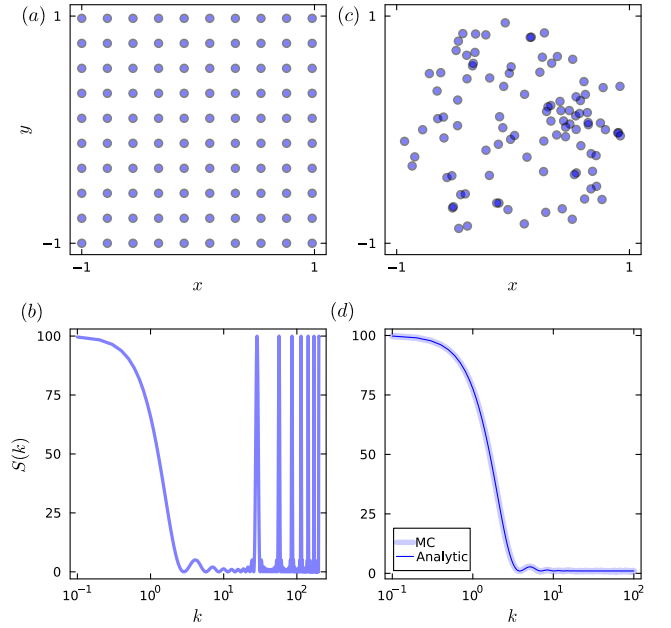


FIG. 1. Structure factor of a point system on a regular lattice and BPP. Panels (a) and (b) show a system of  $N = 100$  points on a square lattice and its corresponding structure factor  $S(\mathbf{k})$ , determined numerically and plotted along  $\mathbf{k} = (k, 0)$ . Panels (c) and (d) depict a specific realization of a BPP with  $N = 100$  points within a unit radius disk, and the structure factor of the corresponding process, plotted along  $\mathbf{k} = (k, 0)$ . In panel (d), the thin solid line represents the analytical expression given by Eq. (4), while the thicker transparent line is obtained by numerically computing  $S(\mathbf{k})$  using a Monte Carlo simulation, averaging over 100 realizations of the process.

Specifically, the characteristic profile of  $S_{\text{BPP}(N)}(\mathbf{k})$ , derived in (4), can serve as a benchmark for assessing the independence and uniformity of point distributions. By comparing the structure factor  $S(\mathbf{k})$  of a generic  $N$ -point process with  $S_{\text{BPP}(N)}(\mathbf{k})$ , any observed deviations can indicate whether the points of the examined process have been sampled uniformly and independently.

In a physical system, excluding the influence of an external potential, such deviations may suggest the presence of inter-particle interactions. However, for a two-dimensional point pattern,  $S(\mathbf{k})$  is generally a two-dimensional function, making the comparison between a given structure factor and the reference somewhat inconvenient. This task becomes even more challenging as the number of spatial dimensions increases. Dimensional reduction is possible for a homogeneous point process on a spherically symmetric domain, where  $S(\mathbf{k})$  depends only on the magnitude of  $\mathbf{k}$ , thus encoding all relevant information in a single dimension. Nevertheless, the structure factor does not, in general, exhibit this symmetry.

This motivated us to introduce a modified version of the structure factor, which we call the distance form factor (DFF),

defined as

$$\text{DFF}(k) := \text{Re} \left\langle \frac{1}{N^2} \sum_{i,j=1}^N e^{ik|\mathbf{r}_i - \mathbf{r}_j|} \right\rangle = \left\langle \frac{1}{N^2} \sum_{i,j=1}^N \cos(|\mathbf{r}_i - \mathbf{r}_j|k) \right\rangle. \quad (5)$$

The main difference from  $S(\mathbf{k})$  is the replacement of the scalar product  $\mathbf{k} \cdot (\mathbf{r}_i - \mathbf{r}_j)$  with  $k|\mathbf{r}_i - \mathbf{r}_j|$ , where  $k$  is a scalar. Consequently, the resulting DFF( $k$ ) is a one-dimensional real function.

The reader may notice the analogy between the DFF, as defined in Eq. (5), and the spectral form factor (SFF). Specifically, given a matrix of dimension  $N$  with eigenvalues denoted by  $E_i$ , the SFF is defined as [36]:

$$\text{SFF}(t) = \frac{1}{N^2} \left\langle \sum_{n,m=1}^N e^{it(E_m - E_n)} \right\rangle, \quad (6)$$

and has been used to study the properties of energy levels in various physical systems, including atomic nuclei, quantum chaotic systems, and black holes [4, 6–9, 37–39]. In this context, the spacing between such eigenvalues plays a crucial role, e.g., in assessing integrability and its breakdown.

In the following section, after presenting the general formal definition of the DFF for a generic spatial point process, we provide its explicit calculation for the BPP and PPP.

### III. DEFINITION AND GENERAL PROPERTIES OF THE DISTANCE FORM FACTOR

#### A. Definition and numerical examples

In a generic spatial point process defined over a domain  $\mathcal{D}$ , an event  $E$  corresponds to a specific arrangement of  $N$  points within  $\mathcal{D}$ :

$$E = \{\mathbf{r}_1, \dots, \mathbf{r}_N\} \quad , \quad \mathbf{r}_i \in \mathcal{D} \quad \forall i. \quad (7)$$

We define the distance form factor of the process as

$$\text{DFF}(k) = \frac{1}{N^2} \left\langle \sum_{i,j=1}^N \cos(|\mathbf{r}_i - \mathbf{r}_j|k) \right\rangle, \quad (8)$$

where the average  $\langle \cdot \rangle$  is performed over all the possible configurations  $E$  of the point system. In particular, denoting by  $\rho(E) := \rho(\mathbf{r}_1, \dots, \mathbf{r}_N)$  the probability density of a certain configuration  $E$ ,

$$\text{DFF}(k) = \frac{1}{N^2} \sum_{i,j=1}^N \left( \int_{\mathcal{D}^N} \cos(|\mathbf{r}_i - \mathbf{r}_j|k) \rho(\mathbf{r}_1, \dots, \mathbf{r}_N) d^N \mathbf{r} \right), \quad (9)$$

where  $d^N \mathbf{r} = d\mathbf{r}_1 \cdots d\mathbf{r}_N$ . The DFF can be used to characterize different classes of point patterns, with its behavior varying according to the salient feature in each class. By way of example, in Fig. 2, the case of a regular square lattice pattern is compared with that of a Penrose tiling as an example of a quasiperiodic pattern [40, 41] and a homogeneous PPP. In all

cases, the DFF exhibits a decay from unit value until a dip and a subsequent steep increase towards a plateau. The presence of spikes in the plateau is characteristic of the regular pattern, which is reduced in the quasiperiodic case and washed out in the random case.

#### B. Relation to the spacing distribution

By separating the terms in Eq. (8) into the cases with  $i = j$  and  $i \neq j$  and applying the linearity of the expectation value, the DFF can be written as

$$\text{DFF}(k) = \frac{1}{N^2} \left( N + \sum_{(i \neq j)=1}^N \langle \cos(|\mathbf{r}_i - \mathbf{r}_j|k) \rangle \right) \quad (10)$$

$$= \frac{1}{N} + \left( 1 - \frac{1}{N} \right) \langle \cos(|\mathbf{r}_1 - \mathbf{r}_2|k) \rangle, \quad (11)$$

where the last line follows from assuming permutation symmetry in the indices. It is then convenient to consider the two-point distance,  $s := |\mathbf{r}_1 - \mathbf{r}_2|$ , in terms of which

$$\langle \cos(|\mathbf{r}_1 - \mathbf{r}_2|k) \rangle := \langle \cos(sk) \rangle = \int_0^{s_{\max}} \cos(sk) P_{\mathcal{D}}(s) ds, \quad (12)$$

where  $P_{\mathcal{D}}(s)$  represents the probability distribution for the distance  $s$  between two points on the domain  $\mathcal{D}$ , with  $s_{\max}$  its maximum value. This transformation reduces the dimension of our problem from  $d$  to 1 by introducing the probability density  $P_{\mathcal{D}}(s)$ .

Thus, the DFF is related to the even Fourier transform of  $P_{\mathcal{D}}(s)$  as

$$\text{DFF}(k) = \frac{1}{N} + \left( 1 - \frac{1}{N} \right) \int_0^{s_{\max}} \cos(sk) P_{\mathcal{D}}(s) ds. \quad (13)$$

Conversely, given the DFF, the expression for the probability  $P_{\mathcal{D}}(s)$  can be retrieved as follows. To this end, we define

$$\mathcal{I}_{\mathcal{D}}(k) := \int_0^{s_{\max}} \cos(sk) P_{\mathcal{D}}(s) ds, \quad (14)$$

multiply both sides of this equation by  $\cos(s'k)$  and integrate over  $k$  to find

$$\int_{-\infty}^{\infty} \mathcal{I}_{\mathcal{D}}(k) \cos(s'k) dk = \int_{-\infty}^{\infty} \int_0^{s_{\max}} \cos(s'k) \cos(sk) P_{\mathcal{D}}(s) dk ds. \quad (15)$$

Using the result

$$\int_{-\infty}^{\infty} \cos(s'k) \cos(sk) dk = \pi(\delta(s + s') + \delta(s - s')), \quad (16)$$

and, assuming that  $0 \leq s' \leq s_{\max}$ , Eq. (15) becomes

$$\int_{-\infty}^{\infty} \mathcal{I}_{\mathcal{D}}(k) \cos(s'k) dk = \pi P_{\mathcal{D}}(s'). \quad (17)$$

Therefore, given the DFF( $k$ ), the inverse transformation to find  $P_{\mathcal{D}}$  is

$$P_{\mathcal{D}}(s) = \frac{N}{\pi(N-1)} \int_{-\infty}^{\infty} \left( \text{DFF}(k) - \frac{1}{N} \right) \cos(sk) dk. \quad (18)$$

Equations (13) and (18) thus establish a direct relation between the DFF and the spacing distribution.

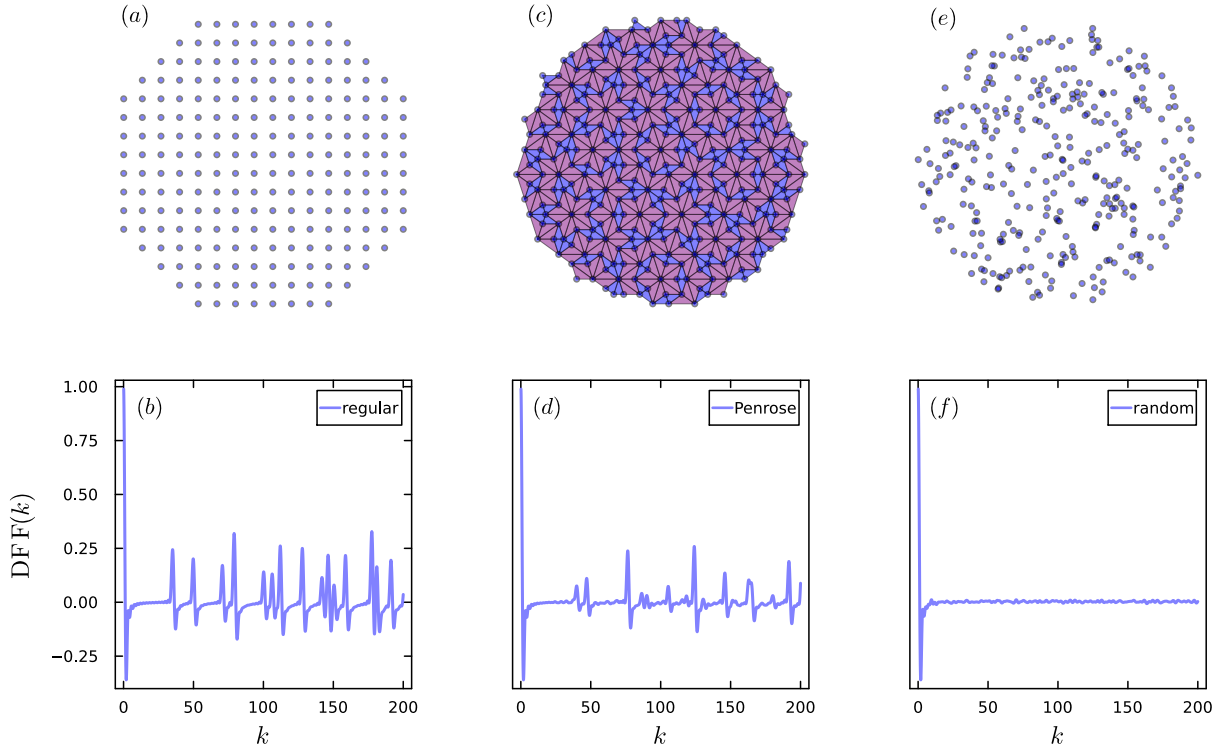


FIG. 2. Distance form factor of various point patterns. Panels (a) and (b) show a regular square lattice and its corresponding DFF, respectively. Panel (c) presents a Penrose tiling (P3), with its corresponding DFF in (d). Panel (e) depicts a single realization of a PPP, with its DFF in (f). In all three cases, the number and density of points are identical.

#### IV. DISTANCE FORM FACTOR FOR BINOMIAL AND POISSON POINT PROCESSES ON A $d$ -DIMENSIONAL BALL

In the following, we focus on the N-BPP defined on a  $d$ -dimensional ball of radius  $R$ ,  $B_d(R) = \{\mathbf{r} \in \mathbb{R}^d : \|\mathbf{r}\| \leq R\}$ . Extending our results to the homogeneous PPP or cases where  $N$  fluctuates according to a generic distribution is straightforward, as it simply requires averaging the results obtained for the BPP case over  $N$ .

Under these assumptions, due to the independence between random points, all the configurations  $E$  are equally likely, with a corresponding probability density fixed by the normalization condition:

$$\rho(E) = \left( \frac{1}{V_{B_d(R)}} \right)^N, \quad (19)$$

where  $V_{B_d(R)}$  is the volume of the  $d$ -dimensional ball:

$$V_{B_d(R)} = \frac{\pi^{\frac{d}{2}}}{\Gamma(\frac{d}{2} + 1)} R^d. \quad (20)$$

We now derive the analytical expression of the DFF in this scenario by explicitly evaluating the average in Eq. (8).

The remaining average in Eq. (11) can be computed by integrating over all possible system configurations, uniformly

weighted according to Eq. (19). This is expressed as

$$\begin{aligned} \langle \cos(|\mathbf{r}_1 - \mathbf{r}_2|k) \rangle &= \left( \frac{1}{V_{B_d(R)}} \right)^N \int_{B_d(R)} \cos(|\mathbf{r}_1 - \mathbf{r}_2|k) d^N \mathbf{r} \\ &= \left( \frac{1}{V_{B_d(R)}} \right)^2 \int_{B_d(R)} \cos(|\mathbf{r}_1 - \mathbf{r}_2|k) d\mathbf{r}_1 d\mathbf{r}_2. \end{aligned} \quad (21)$$

However, it reveals more convenient to make use of Eq. (12), identifying the corresponding  $P_{\mathcal{D}}(s)$  with the probability distribution  $P_d(s)$  for the distance  $s$  between two independent and uniformly distributed random points on a  $d$ -dimensional ball. The expression for  $P_d(s)$  is known from the Ball Line Picking problem in stochastic geometry, and it is given by [42, 43]

$$P_d(s) = \frac{d \cdot s^{d-1}}{R^d} I_{1-\frac{s^2}{4R^2}} \left( \frac{d+1}{2}, \frac{1}{2} \right), \quad (22)$$

where  $I_z(a, b)$  is the regularized Beta function, defined in terms of the incomplete beta function  $B(z; a, b)$  and the beta function  $B(a, b)$  as [44]

$$I_z(a, b) := \frac{B(z; a, b)}{B(a, b)}. \quad (23)$$

We recall the integral representation of  $B(z; a, b)$ , given by

$$B(z; a, b) = \int_0^z u^{a-1} (1-u)^{b-1} du. \quad (24)$$

Furthermore,  $B(a, b)$  can be expressed in terms of the Gamma function as

$$B(a, b) = \frac{\Gamma(a)\Gamma(b)}{\Gamma(a+b)}. \quad (25)$$

By making use of equations (23), (24) and (25), we can write  $P_d(s)$  in the form

$$P_d(s) = \frac{d \cdot s^{d-1}}{R^d} \frac{\Gamma(\frac{d}{2} + 1)}{\Gamma(\frac{d+1}{2})\Gamma(\frac{1}{2})} \int_0^{1-\frac{s^2}{4R^2}} u^{\frac{d-1}{2}} (1-u)^{-\frac{1}{2}} du. \quad (26)$$

After plugging Eq. (26) into Eq. (12), one is left to evaluate the integral

$$\begin{aligned} \mathcal{I}_d(k) &:= \int_0^{2R} \cos(sk) P_d(s) ds \\ &= \frac{d}{R^d} \frac{\Gamma(\frac{d}{2} + 1)}{\Gamma(\frac{d+1}{2})\Gamma(\frac{1}{2})} \\ &\quad \times \int_0^{2R} \cos(sk) s^{d-1} \left[ \int_0^{1-\frac{s^2}{4R^2}} u^{\frac{d-1}{2}} (1-u)^{-\frac{1}{2}} du \right] ds. \end{aligned} \quad (27)$$

To ease the notation, let  $g(s)$  represent the integral inside the square bracket in Eq. (27),

$$g(s) := \int_0^{1-\frac{s^2}{4R^2}} u^{\frac{d-1}{2}} (1-u)^{-\frac{1}{2}} du, \quad (28)$$

so that we can more compactly write

$$\mathcal{I}_d(k) = \frac{d}{R^d} \frac{\Gamma(\frac{d}{2} + 1)}{\Gamma(\frac{d+1}{2})\Gamma(\frac{1}{2})} \int_0^{2R} \cos(sk) s^{d-1} g(s) ds. \quad (29)$$

We will now proceed by integration by parts. Let us first denote with  $G(s)$  the primitive of  $s^{d-1} \cos(sk)$ , which can be computed explicitly in terms of the hypergeometric function  ${}_1F_2$  [44, 45] as

$$G(s) := \int_0^s x^{d-1} \cos(xk) dx = \frac{s^d}{d} {}_1F_2\left(\frac{d}{2}; \frac{1}{2}, 1 + \frac{d}{2}; -\frac{1}{4}k^2 s^2\right). \quad (30)$$

Integrating  $\mathcal{I}_d$  by parts then yields

$$\begin{aligned} \mathcal{I}_d &= \frac{d}{R^d} \frac{\Gamma(\frac{d}{2} + 1)}{\Gamma(\frac{d+1}{2})\Gamma(\frac{1}{2})} \left( [G(s)g(s)]_0^{2R} - \int_0^{2R} G(s)g'(s) ds \right) \\ &= -\frac{d}{R^d} \frac{\Gamma(\frac{d}{2} + 1)}{\Gamma(\frac{d+1}{2})\Gamma(\frac{1}{2})} \int_0^{2R} G(s)g'(s) ds, \end{aligned} \quad (31)$$

where, to get to the last line, we used  $G(0) = 0$  and  $g(2R) = 0$ . Furthermore, the derivative of  $g(s)$  can be evaluated via the fundamental theorem of calculus,

$$\frac{d}{dx} \left( \int_0^{h(x)} f(u) du \right) = f(h(x))h'(x). \quad (32)$$

In particular,

$$g'(s) = -\frac{1}{R} \left( 1 - \frac{s^2}{4R^2} \right)^{\frac{d-1}{2}}. \quad (33)$$

We can then plug the explicit expressions for  $G(s)$  and  $g'(s)$ , respectively given in Eq. (30) and Eq. (33), into Eq. (31) and perform the remaining integration to find

$$\begin{aligned} \mathcal{I}_d &= \frac{1}{R^{d+1}} \frac{\Gamma(\frac{d}{2} + 1)}{\Gamma(\frac{d+1}{2})\Gamma(\frac{1}{2})} \\ &\quad \times \int_0^{2R} s^d {}_1F_2\left(\frac{d}{2}; \frac{1}{2}, 1 + \frac{d}{2}; -\frac{1}{4}k^2 s^2\right) \left( 1 - \frac{s^2}{4R^2} \right)^{\frac{d-1}{2}} ds \\ &= \frac{1}{R^{d+1}} \frac{\Gamma(\frac{d}{2} + 1)}{\Gamma(\frac{d+1}{2})\Gamma(\frac{1}{2})} \pi R^{d+1} \Gamma(d+1) \Gamma\left(\frac{d+1}{2}\right) \\ &\quad \times {}_2F_3\left(\frac{d+1}{2}, \frac{d}{2}; \frac{1}{2}, \frac{d+2}{2}, d+1; -k^2 R^2\right) \\ &= \sqrt{\pi} (d!) \Gamma\left(\frac{d}{2} + 1\right) {}_2F_3\left(\frac{d+1}{2}, \frac{d}{2}; \frac{1}{2}, \frac{d+2}{2}, d+1; -k^2 R^2\right), \end{aligned} \quad (34)$$

where we used the following properties of the Gamma function:

$$\Gamma\left(\frac{1}{2}\right) = \sqrt{\pi}, \quad \Gamma(d) \cdot d = d!. \quad (35)$$

The resulting expression for  $\mathcal{I}_d$  in (34) can be further simplified by recalling the definition of the hypergeometric regularized function  ${}_2\tilde{F}_3$  in terms of the standard  ${}_2F_3$  [44],

$${}_2\tilde{F}_3(a_1, a_2; b_1, b_2, b_3; z) := \frac{{}_2F_3(a_1, a_2; b_1, b_2, b_3; z)}{\Gamma(b_1)\Gamma(b_2)\Gamma(b_3)}. \quad (36)$$

Therefore,

$$\begin{aligned} \mathcal{I}_d &= \frac{\sqrt{\pi} (d!) \Gamma\left(\frac{d}{2} + 1\right)}{\Gamma\left(\frac{1}{2}\right) \Gamma\left(\frac{d+2}{2}\right) \Gamma(d+1)} {}_2F_3\left(\frac{d+1}{2}, \frac{d}{2}; \frac{1}{2}, \frac{d+2}{2}, d+1; -k^2 R^2\right) \\ &= {}_2F_3\left(\frac{d+1}{2}, \frac{d}{2}; \frac{1}{2}, \frac{d+2}{2}, d+1; -k^2 R^2\right), \end{aligned} \quad (37)$$

where we made again use of the properties (35).

Finally, by plugging the result of Eq. (37) in Eq. (11), the expression for the DFF reads

$$\text{DFF}(k) = \frac{1}{N} + \left( 1 - \frac{1}{N} \right) {}_2F_3\left(\frac{d+1}{2}, \frac{d}{2}; \frac{1}{2}, \frac{d+2}{2}, d+1; -k^2 R^2\right), \quad (38)$$

which constitutes our main result for the BPP. As previously mentioned, extending Eq. (38) to cases where  $N$  fluctuates across different trials according to a generic distribution is straightforward and involves averaging the expression (38) over  $N$ . Special care is only required when dealing with the case  $N = 0$ , as the DFF is not well-defined in this scenario. To

address this, we conventionally assign a value of 0 to the DFF when  $N = 0$ . In particular, for a homogeneous PPP we have:

$$\begin{aligned} \text{DFF}_{\text{PPP}}(k) &= f(\lambda) + (1 - f(\lambda)) \\ &\times {}_2F_3\left(\frac{d+1}{2}, \frac{d}{2}; \frac{1}{2}, \frac{d+2}{2}, d+1; -k^2 R^2\right), \end{aligned} \quad (39)$$

where  $\lambda$  is the intensity of the PPP over  $B_d(R)$  and

$$f(\lambda) = e^{-\lambda} (-\gamma + \text{Chi}(\lambda) - \log(\lambda) + \text{Shi}(\lambda)), \quad (40)$$

where  $\text{Chi}(\lambda)$  and  $\text{Shi}(\lambda)$  are respectively the hyperbolic cosine and sine integrals [44], and  $\gamma$  the Euler-Mascheroni constant.

In the next subsection, we consider general features of the DFF, as well as some special cases of Eq. (38) and discuss connections with random matrix theory.

## V. CHARACTERIZATION OF THE DISTANCE FORM FACTOR FOR STOCHASTIC POINT PROCESSES

### A. Asymptotics, special cases and connections to quantum chaos

A Taylor series expansion of the DFF (38) for a BPP around  $kR = 0$  yields

$$\text{DFF}(k) = 1 - \frac{(N-1)d}{N(d+2)}(kR)^2 + \frac{d(d+3)(N-1)}{6N(d+4)(d+2)}(kR)^4 + \mathcal{O}(k^6 R^6), \quad (41)$$

indicating a quadratic decay from unit value for small values of  $kR$  that is interrupted around

$$kR \approx \sqrt{6 + \frac{6}{3+d}}, \quad (42)$$

that is independent of  $N$ . Furthermore, from the Riemann–Lebesgue lemma, it follows that  $\mathcal{I}_d$  vanishes for large values of  $kR$ , so that

$$\text{DFF}(k) \sim \frac{1}{N}. \quad (43)$$

Thus, the DFF is expected to exhibit a decay from unit value, forming a dip, with subsequent growth leading to a plateau, as anticipated by the numerical examples in Sec. III.

The special cases of our formula (38) for dimensions 1, 2, and 3 are explicitly presented in Table (V A), with the corresponding plots shown in Fig. 3.

What stands out is the characteristic structure of sub-figures 3(b) and (c), consisting of a dip followed by a ramp and a subsequent plateau. The observed behavior is consistent with the short and long  $k$  asymptotic.

The behavior of the DFF is reminiscent of that in the spectral form factor in quantum chaotic systems. Quantum chaos manifests in correlations between the eigenvalues of an isolated Hamiltonian quantum system [4]. Its characterization often relies on the eigenvalue spacing distribution. The absence of degeneracies in the energy spectrum leads to a suppression of the probability of finding a pair of eigenvalues at

vanishing spacing, known as the correlation hole. Spectral signatures can be conveniently revealed by analyzing the spectral form factor, which is the average of the absolute value of the Fourier transform of the eigenvalue density [6–9]. The spectral form factor exhibits a short-time decay from unit value, forming a dip and a subsequent ramp before saturating at a plateau [4, 37, 38].

It might appear surprising that the DFF of a BPP, where the random points are uncorrelated, shares this behavior. However, this is purely a geometrical effect due to the dimension of the domain space, which introduces a fictitious repulsion between points. In fact, as the space dimension increases, it becomes increasingly rare to sample points close to each other. This heuristic statement is mathematically encoded in the nearest neighbor spacing distribution. For a BPP on a  $d$ -dimensional ball, this distribution is given by [4]

$$P_d^{\text{NN}}(s) = \alpha ds^{d-1} e^{-\alpha s^d}, \quad (44)$$

with further details discussed in Sec. V B. For  $d = 2$ , it simplifies to the well-known Wigner-Dyson distribution:

$$P_2^{\text{NN}}(s) = \frac{\pi}{2} s e^{-\frac{\pi^2}{4} s^2}. \quad (45)$$

This distribution is ubiquitous in the study of quantum chaos, where  $S$  denotes the eigenvalue spacing [4, 36, 46], and also characterizes the spatial patterns of topological defects generated in crossing a continuous phase transition [32, 33].

In the limit  $s \rightarrow 0$ , for  $d > 1$ , (44) goes to zero, indicating the presence of an effect analogous to the energy level repulsion in the spectral statistics of disordered quantum systems, which leads to the presence of the correlation hole. This explains why this feature is absent in Fig. 3(a), corresponding to the  $1d$  case. In fact, in that scenario, the nearest neighbor spacing distribution is Poissonian,

$$P_1^{\text{NN}}(s) = e^{-s}, \quad (46)$$

which does not vanish in the small spacing limit, resulting in the absence of the correlation hole.

### B. Distance form factor decomposition

The DFF contains information on the spacing between any pair of points of the process. It is in fact, up to constant factors, the Fourier transform of the spacing distribution  $P_d(s)$ , as it is apparent from Eq. (12). However, it is possible to separate the contributions to  $\text{DFF}(k)$  based on the neighborhood degree between pairs of points. This is analogous to the decomposition recently put forward in the canonical spectral form factor in the context of quantum chaos [39]. In particular, we have

$$\text{DFF}(k) = \frac{1}{N} + \sum_{n=1}^{N-1} \text{DFF}^{(n)}(k), \quad (47)$$

where  $\text{DFF}^{(n)}(k)$  denotes the distance form factor computed considering only  $n$ -th nearest neighboring points. Specifically,

$$\text{DFF}^{(n)}(k) := \frac{1}{N^2} \left\langle \sum_{i=1}^N \cos(|\mathbf{r}_i - \mathbf{r}_{n^{\text{th}}(i)}|k) \right\rangle, \quad (48)$$

	$\mathcal{I}_d$
$d = 1$	$\frac{\sin^2(kR)}{(kR)^2}$
$d = 2$	$\frac{-2kR(1 + 2J_0(2kR)) + 6J_1(2kR)}{k^3 R^3}$
$d = 3$	$\frac{9(3k^2 R^2 + 2kR(k^2 R^2 - 5)\sin(2kR) + (7k^2 R^2 - 5)\cos(2kR) + 5)}{2k^6 R^6}$

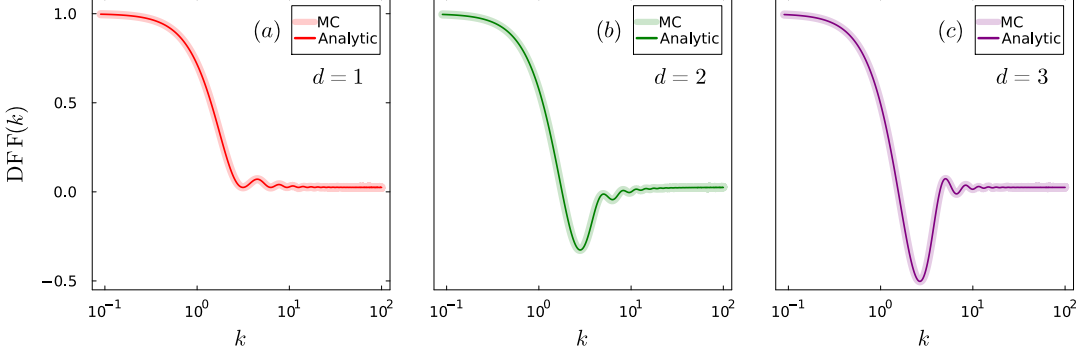


FIG. 3. Distance form factor of a BPP on a  $d$ -dimensional ball with unit radius. Panels (a), (b), and (c) correspond respectively to  $d = 1, 2, 3$ . In each of the three cases, the solid thin line represents the analytic expression given in Eq. (38), while the transparent thicker line corresponds to the DFF computed numerically in a Monte Carlo simulation with  $N = 40$  points, averaging over 300 randomly generated configurations.

with  $\mathbf{r}_{n^{\text{th}}(i)}$  representing the position of the  $n$ -th closest point to the point at  $\mathbf{r}_i$ .

While there is an analogy with the decomposition of the spectral form factor, we emphasize an important difference here. In the spectral form factor, the  $n$ -th nearest neighbor of the  $i$ -th energy level is defined as the  $(i + n)$ -th level, assuming the levels are ordered, with their spacing given by  $s_i^{(n)} = E_{i+n} - E_i$  [39]. In contrast, for the distance form factor, the energy levels are replaced by the positions of the points. Thus, although the neighbor definition from the spectral form factor can still be applied in a one-dimensional point process, the natural ordering that makes this possible is lost in higher dimensions.

Equation (48) can be further rewritten as

$$\text{DFF}^{(n)}(k) = \frac{1}{N} \int_0^{2R} \cos(sk) P_d^{(n)}(s) ds, \quad (49)$$

with  $P_d^{(n)}$  the  $n$ -th nearest neighbor spacing probability density. In the limit where the number of points  $N \rightarrow \infty$ , and provided that we rescale the spacing  $s$  with the mean  $n$ -th nearest neighbor spacing distance  $\langle s^{(n)} \rangle$  ( $s \rightarrow \frac{s}{\langle s^{(n)} \rangle} =: S$ ), such probability assumes the simple form [4]

$$P_d^{(n)}(s) ds \rightarrow P_d^{(n)}(S) dS = \frac{\alpha^n}{(n-1)!} S^{(dn-1)} e^{-S^d \alpha} dS, \quad (50)$$

where  $\alpha := \frac{\Gamma^d(\frac{1}{d} + n)}{\Gamma^d(n)}$ , and the explicit expression for  $\langle s^{(n)} \rangle$  is given by

$$\langle s^{(n)} \rangle = \frac{R \Gamma(\frac{1}{d} + n)}{N^{\frac{1}{d}} \Gamma(n)}. \quad (51)$$

Using Eq. (50) we can then compute the large  $N$  limit of  $\text{DFF}^{(n)}(k)$ , which reads

$$\begin{aligned} \text{DFF}^{(n)}(k) &= \frac{1}{N} \int_0^\infty \cos(\langle s^{(n)} \rangle S k) P_d^{(n)}(S) dS \\ &= \frac{\alpha^n d}{N(n-1)!} \int_0^\infty \cos\left(\frac{\rho \Gamma(\frac{1}{d} + n)}{\Gamma(n)} S k\right) S^{(dn-1)} e^{-S^d \alpha} dS \\ &= \frac{d}{N(n-1)!} \int_0^\infty \cos(\rho k x) x^{(dn-1)} e^{-x^d} dx, \end{aligned} \quad (52)$$

where we have defined the ratio  $\rho := \frac{R}{N^{\frac{1}{d}}}$ , and, in the last line, we have performed the change of variables  $x = S^{\frac{1}{d}}$ . The closed result in (52), valid for  $n \ll N$ , is explicitly given for some important special cases in Table I.

	$\text{DFF}^{(n)}(k)$
$d = 1$	$\frac{1}{N} (k^2 \rho^2 + 1)^{-\frac{n}{2}} \cos(n \arctan(k\rho))$
$d = 2$	$\frac{1}{N} {}_1F_1\left(n, \frac{1}{2}; -\frac{k^2 \rho^2}{4}\right)$

TABLE I. The  $n$ -th component of the DFF  $\text{DFF}^{(n)}(k)$  for a BPP of  $N$  points on a line ( $d = 1$ ), and on a disk ( $d = 2$ ). The factor  $\rho$  is defined as the ratio  $\frac{R}{N^{\frac{1}{d}}}$ . The expressions are valid in the large  $N$  limit.

As a remark, we note that the one-dimensional DFF and its decomposition can be equivalently mapped onto the spectral

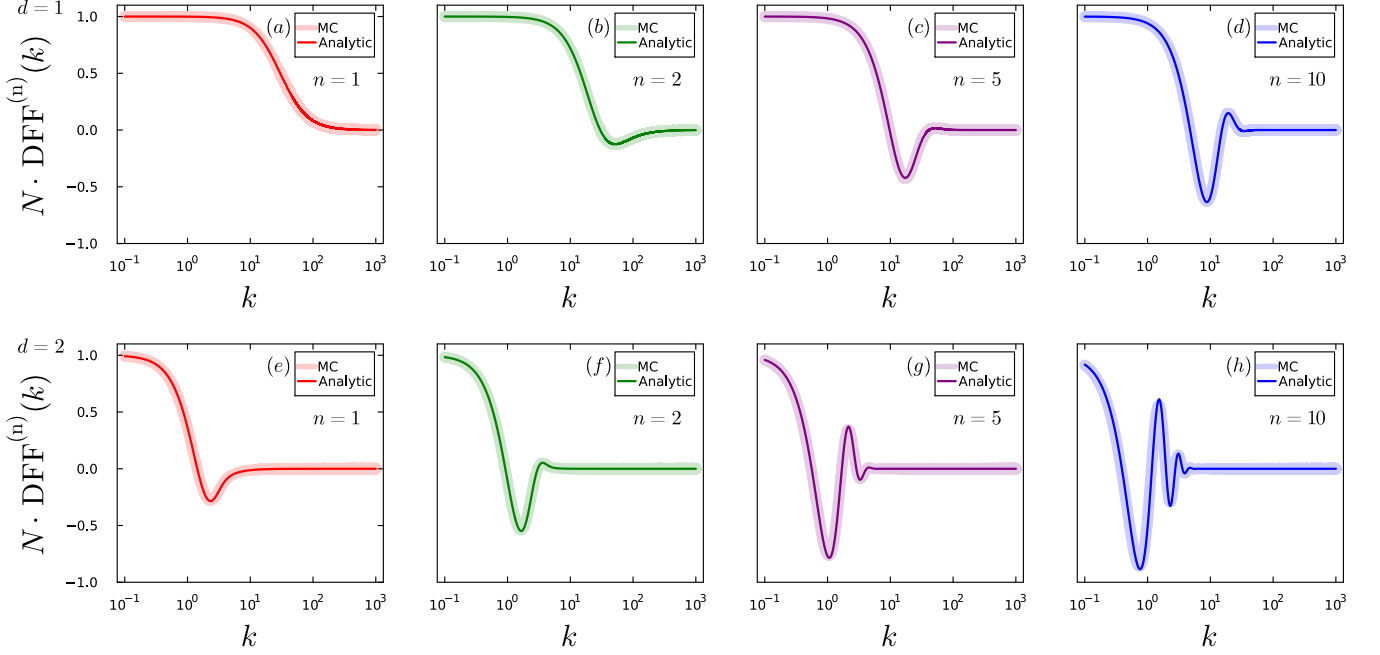


FIG. 4. Different components of the DFF for a BPP of  $N = 1500$  points. Panels (a), (b), (c) and (d) correspond respectively to the first, second, fifth and tenth component of the DFF for the 1D process on a segment of length  $2R = 100$ . Panels (e), (f), (g) and (h) show the same components of the DFF for the 2D process on a disk of radius  $R = 50$ . In all cases, the thin solid line corresponds to the analytical expression provided in Table (I), while the thick transparent line corresponds to the  $\text{DFF}^{(n)}$  computed numerically by a Monte Carlo simulation, averaging over 300 trials. For convenience, in all the panels, we have plotted the rescaled  $\text{DFF}^{(n)}$  with the total number of points.

form factor (SFF) of an integrable system, where the energy level spacings follow Poissonian statistics [39]. The difference between the components of the SFF and DFF is solely in the pre-factor, which arises from the different definitions of neighbors previously discussed. The correspondence extends to certain components of SFF for random matrices from Gaussian ensembles (GOE, GUE, GSE) and the components of DFF for a PPP in 2D. This is due to the equivalence between the spacing distributions of the  $n$ -th nearest neighboring eigenvalues in Gaussian ensembles and those in a two-dimensional PPP [10].

For completeness, we also report the expression for  $\text{DFF}^{(n)}(k)$  in dimensions  $d = 3$ , which reads

$$\begin{aligned} \text{DFF}_{d=3}^{(n)}(k) &= \frac{1}{N(n-1)!} \left[ \Gamma(n) {}_2F_5 \left( \frac{n}{2} + \frac{1}{2}, \frac{n}{2}; \frac{1}{6}, \frac{1}{3}, \frac{1}{2}, \frac{2}{3}, \frac{5}{6}; -\frac{\rho^6 k^6}{11664} \right) \right. \\ &+ \frac{\rho^4 k^4}{24} \Gamma \left( n + \frac{4}{3} \right) {}_2F_5 \left( \frac{n}{2} + \frac{2}{3}, \frac{n}{2} + \frac{7}{6}; \frac{5}{6}, \frac{7}{6}, \frac{4}{3}, \frac{3}{2}, \frac{5}{3}; -\frac{\rho^6 k^6}{11664} \right) \\ &\left. - \frac{\rho^2 k^2}{2} \Gamma \left( n + \frac{2}{3} \right) {}_2F_5 \left( \frac{n}{2} + \frac{1}{3}, \frac{n}{2} + \frac{5}{6}; \frac{1}{2}, \frac{2}{3}, \frac{5}{6}, \frac{7}{6}, \frac{4}{3}; -\frac{\rho^6 k^6}{11664} \right) \right]. \end{aligned} \quad (53)$$

### C. The infinite-dimensional limit

We close this section by reporting a simple corollary obtained by considering the limit  $d \rightarrow \infty$  of the DFF expression given in Eq. (38). In particular, let us compute

$$\begin{aligned} \mathcal{I}_\infty(k) &:= \lim_{d \rightarrow \infty} \mathcal{I}_d(k) \\ &= \lim_{d \rightarrow \infty} {}_2F_3 \left( \frac{d+1}{2}, \frac{d}{2}; \frac{1}{2}, \frac{d+2}{2}, d+1; -k^2 R^2 \right). \end{aligned} \quad (54)$$

By using the series representation of the hypergeometric function [45], the limit takes the form

$$\mathcal{I}_\infty(k) = \lim_{d \rightarrow \infty} \sum_{n=0}^{\infty} \frac{\left(\frac{d+1}{2}\right)_n \left(\frac{d}{2}\right)_n}{\left(\frac{1}{2}\right)_n \left(\frac{d+2}{2}\right)_n (d+1)_n} \frac{(-k^2 R^2)^n}{n!}, \quad (55)$$

where  $(x)_n$  is the Pochhammer's symbol, defined as [44]

$$(x)_n = x(x+1) \cdots (x+n-1). \quad (56)$$

In Eq. (55), it is possible to interchange the limit with the infinite summation by virtue of Tannery's theorem [47]. To apply the theorem, it is sufficient to prove that

$$\left| \frac{\left(\frac{d+1}{2}\right)_n \left(\frac{d}{2}\right)_n}{\left(\frac{1}{2}\right)_n \left(\frac{d+2}{2}\right)_n (d+1)_n} \frac{(-k^2 R^2)^n}{n!} \right| \leq M_n \quad \text{and} \quad \sum_{n=0}^{\infty} M_n < \infty, \quad (57)$$

with  $M$  independent of  $d$ . The bound is achieved by

$$\left| \frac{\left(\frac{d+1}{2}\right)_n \left(\frac{d}{2}\right)_n}{\left(\frac{1}{2}\right)_n \left(\frac{d+2}{2}\right)_n (d+1)_n} \frac{(-k^2 R^2)^n}{n!} \right| \leq \frac{2(k^2 R^2)^n}{n!} \quad (58)$$

and

$$\sum_{n=0}^{\infty} \frac{2(k^2 R^2)^n}{n!} = 2e^{k^2 R^2} < \infty. \quad (59)$$

Therefore, given that

$$\lim_{d \rightarrow \infty} \frac{\left(\frac{d+1}{2}\right)_n \left(\frac{d}{2}\right)_n}{\left(\frac{1}{2}\right)_n \left(\frac{d+2}{2}\right)_n (d+1)_n} = \frac{2^{-n}}{\left(\frac{1}{2}\right)_n}, \quad (60)$$

bringing the limit inside the sum in Eq. (55), we obtain

$$\mathcal{I}_{\infty}(k) = \sum_{n=0}^{\infty} \frac{2^{-n}}{\left(\frac{1}{2}\right)_n} \frac{(-k^2 R^2)^n}{n!} = \cos(\sqrt{2}kR). \quad (61)$$

Recalling the definition of  $\mathcal{I}_d$  from Eq. (27), one finds the following equality, valid in the  $d \rightarrow \infty$  limit:

$$\begin{aligned} \langle \cos(ks) \rangle &= \cos(\sqrt{2}kR) \\ \Rightarrow \sum_{n=0}^{\infty} \frac{(-1)^n k^{2n}}{(2n)!} \langle s^{2n} \rangle &= \sum_{n=0}^{\infty} \frac{(-1)^n k^{2n} (\sqrt{2}R)^{2n}}{(2n)!}. \end{aligned} \quad (62)$$

By repeatedly taking derivatives with respect to  $k$  on both sides of Eq. (62) and evaluating it at  $k = 0$ , we see that

$$\langle s^{2n} \rangle = (\sqrt{2}R)^{2n}, \quad n \in \mathbb{N}. \quad (63)$$

Equation (63) provides the limit of all even moments of the distance between two random, uniformly distributed, and independent points sampled within a  $d$ -ball as  $d$  approaches infinity. A similar derivation, using the sine function instead of the cosine to define the DFF, leads to the odd moments of the distance:

$$\langle s^{2n+1} \rangle = (\sqrt{2}R)^{2n+1}, \quad n \in \mathbb{N}. \quad (64)$$

In this case, it can be shown that the moments completely determine the probability distribution given that (see [48], p. 514),

$$\lim_{n \rightarrow \infty} \sup \frac{1}{n} \langle s^n \rangle^{\frac{1}{n}} = 0 < \infty. \quad (65)$$

The distance distribution when  $d \rightarrow \infty$  is the Dirac delta function

$$P_{\infty}(s) = \delta(s - \sqrt{2}R), \quad (66)$$

which indicates a concentration of measure, with the suppression of statistical fluctuations.

## VI. DISTANCE FORM FACTOR OF A COULOMB GAS

Up to this point, we have primarily focused on the DFF of Poissonian point processes, where points are sampled independently of each other. This independence can be interpreted as the absence of interaction between the points, making this scenario a model for systems of non-interacting particles. Consequently, the probability density of any given point configuration is separable into the product of the individual probability densities corresponding to each point. A natural generalization is to extend the analysis to point processes where interactions are present. A notable example is given by a system of points subject to Coulomb interaction [49]. In this section, we investigate the DFF in such a setting.

Let us consider, as before, a set of  $N$  points with positions denoted by  $(\mathbf{r}_1, \dots, \mathbf{r}_N)$ , defined over a generic domain  $\mathcal{D}$ . In addition, each point carries an electric charge  $q = \pm 1$ . The Coulomb interaction between any pair of points at positions  $\mathbf{r}_i$  and  $\mathbf{r}_j$ , with respective charges  $q_i$  and  $q_j$ , is given by the pair potential:

$$V(\mathbf{r}_i, \mathbf{r}_j) = \begin{cases} -q_i q_j |\mathbf{r}_i - \mathbf{r}_j| & d = 1, \\ -q_i q_j \log(|\mathbf{r}_i - \mathbf{r}_j|) & d = 2, \\ q_i q_j \frac{1}{|\mathbf{r}_i - \mathbf{r}_j|^{d-2}} & d > 2. \end{cases} \quad (67)$$

Due to the interaction described by (67), if all the points in the system have the same charge, they will repel each other and eventually escape to infinity. To prevent this, an additional confining external potential  $V_{\text{ext}}$  is applied. A typical choice for  $V_{\text{ext}}$  is a harmonic trap. This choice also arises naturally in the  $d = 2$  case in the discussion of log gases in relation to random matrix theory [46]. It also arises in  $d = 1$  in the characterization of the ground-state density of many-body quantum models such as the long-range Lieb-Liniger Hamiltonian [50, 51] and related diffusion models [52]. In our study, we employ a box trap potential to preserve the homogeneity of the system.

The probability density of a certain  $N$ -point configuration is known from the canonical ensemble in statistical mechanics and given by the Gibbs measure [53]

$$P(\mathbf{r}_1, \dots, \mathbf{r}_N) = \frac{1}{\mathcal{Z}} e^{-\frac{\beta}{2} \sum_{i \neq j=1}^N V(\mathbf{r}_i, \mathbf{r}_j)}, \quad (68)$$

where  $\beta$  plays the role of the inverse temperature of the system, and  $\mathcal{Z}$  is the classical canonical partition function

$$\mathcal{Z} = \int_{\mathcal{D}^N} e^{-\frac{\beta}{2} \sum_{i \neq j=1}^N V(\mathbf{r}_i, \mathbf{r}_j)} d^N \mathbf{r}. \quad (69)$$

The distance form factor for a system of points with interaction (67) is given by

$$\begin{aligned} \text{DFF}(k) &= \frac{1}{N^2} \left\langle \sum_{i,j=1}^N \cos(|\mathbf{r}_i - \mathbf{r}_j|k) \right\rangle \\ &= \frac{1}{N^2} \left( N + \frac{1}{\mathcal{Z}} \int_{\mathcal{D}^N} \sum_{i \neq j=1}^N \cos(|\mathbf{r}_i - \mathbf{r}_j|k) e^{-\frac{\beta}{2} \sum_{n \neq m=1}^N V(\mathbf{r}_n, \mathbf{r}_m)} d^N \mathbf{r} \right). \end{aligned} \quad (70)$$

Obtaining a closed form of (70) is generally challenging. Therefore, in the following subsection, we concentrate on the one-dimensional case and assume the regime  $\beta \rightarrow 0$  (high-temperature limit) to determine the first-order correction to the DFF. In the subsequent subsection, we investigate the DFF for the Coulomb gas in higher dimensions using Monte Carlo simulations.

### A. Low $\beta$ expansion of the distance form factor of a 1d Coulomb gas

Let us consider a 1d Coulomb gas confined on the segment  $[-R, R]$ . For now, we assume that the system consists of  $N$  particles, with  $N_+$  positively charged and  $N_- = N - N_+$  negatively charged, all with equal magnitude  $q = |q_n|$ . The DFF of the system, according to Eq. (70), is given by

$$\text{DFF}(k) = \frac{1}{N^2} \left( N + \frac{1}{\mathcal{Z}} C(k, \beta) \right), \quad (71)$$

where, to simplify the expression, we have defined  $C(k, \beta)$  as

$$C(k, \beta) = \int_{[-R, R]^N} \sum_{i \neq j} \cos(|x_i - x_j|k) e^{\frac{\beta}{2} (\sum_{n \neq m} q_n q_m |x_n - x_m|)} d^N x \quad (72)$$

The indices  $(i, j)$  and  $(n, m)$  range from 1 to  $N$ , but this has been omitted here and in what follows for brevity.

We now consider the regime  $\beta \rightarrow 0$  and compute the linear correction in  $\beta$  to the DFF. In particular, we expand the partition function  $\mathcal{Z}$ , defined in Eq. (69), as

$$\begin{aligned} \mathcal{Z} &= \int_{[-R, R]^N} \left( 1 + \frac{\beta}{2} \sum_{i \neq j} q_i q_j |x_i - x_j| \right) d^N x + O(\beta^2) \\ &= (2R)^N + \beta (P_+ - P_-) q^2 (2R)^{N-2} \\ &\quad \times \int_{[-R, R]^2} |x_1 - x_2| dx_1 dx_2 + O(\beta^2) \\ &= (2R)^N + \beta (P_+ - P_-) q^2 (2R)^{(N-2)} \frac{8}{3} R^3 + O(\beta^2), \end{aligned} \quad (73)$$

where  $P_+$  denotes the number of particle pairs with the same charge sign, and  $P_-$  the number of pairs with opposite charges. Specifically,

$$P_+ = \binom{N_+}{2} + \binom{N_-}{2}, \quad P_- = N_+ N_-. \quad (74)$$

Consequently,  $\mathcal{Z}^{-1}$  is given by

$$\frac{1}{\mathcal{Z}} = \frac{1}{(2R)^N} \left( 1 - \frac{2}{3} q^2 R (P_+ - P_-) \beta \right) + O(\beta^2). \quad (75)$$

Let us now carry out the same expansion for  $C(k, \beta)$ :

$$\begin{aligned} C(k, \beta) &= \int_{[-R, R]^N} \sum_{i \neq j} \cos(|x_i - x_j|k) \\ &\quad \times \left( 1 + \frac{\beta}{2} \sum_{n \neq m} q_n q_m |x_n - x_m| + O(\beta^2) \right) d^N x \\ &= \left( N(N-1)(2R)^{N-2} \int_{-R}^R \int_{-R}^R \cos(|x_1 - x_2|k) dx_1 dx_2 \right) \\ &\quad + \frac{\beta}{2} \left( \int_{[-R, R]^N} \sum_{\substack{i \neq j \\ n \neq m}} \cos(|x_i - x_j|k) q_n q_m |x_n - x_m| d^N x \right) + O(\beta^2). \end{aligned} \quad (76)$$

The integral in the first parentheses of Eq. (76) can be readily computed,

$$\begin{aligned} &N(N-1)(2R)^{N-2} \int_{-R}^R \int_{-R}^R \cos(|x_1 - x_2|k) dx_1 dx_2 \\ &= N(N-1)(2R)^{(N-2)} \frac{4 \sin^2(kR)}{k^2}. \end{aligned} \quad (77)$$

We then focus on the term linear in  $\beta$ , which appears in the final line of Eq. (76). This term can be decomposed into three distinct contributions, representing different scenarios for the index pairs. Specifically, in the expression  $\cos(|x_i - x_j|k) |x_n - x_m|$ , the index pairs  $(i, j)$  and  $(n, m)$  can either share both indices, one index, or none. To ease the notation, we define

$$f_{i,j,n,m}(k) := \int_{[-R, R]^N} \cos(|x_i - x_j|k) q_n q_m |x_n - x_m| d^N x. \quad (78)$$

Thus, the term inside the parenthesis in the final line of Eq. (76) can be rewritten as

$$\begin{aligned} &\sum_{i \neq j, n \neq m} f_{i,j,n,m}(k) \\ &= \underbrace{\sum_{\substack{i \neq j, n \neq m \\ |(i,j) \cap (n,m)|=2}} f_{i,j,n,m}(k)}_{a(k)} + \underbrace{\sum_{\substack{i \neq j, n \neq m \\ |(i,j) \cap (n,m)|=1}} f_{i,j,n,m}(k)}_{b(k)} + \underbrace{\sum_{\substack{i \neq j, n \neq m \\ |(i,j) \cap (n,m)|=0}} f_{i,j,n,m}(k)}_{c(k)} \end{aligned} \quad (79)$$

Let us now compute  $a$ ,  $b$  and  $c$  from Eq. (79). First,

$$\begin{aligned} a(k) &= (2R)^{(N-2)} 4(P_+ - P_-) q^2 \\ &\quad \times \int_{[-R, R]^2} \cos(|x_1 - x_2|k) |x_1 - x_2| dx_1 dx_2 \\ &= (2R)^{(N-2)} 4(P_+ - P_-) q^2 \frac{8 \cos^2(kR) [-kR + \tan(kR)]}{k^3}. \end{aligned} \quad (80)$$

The prefactor  $4(P_+ - P_-)$  arises for the following reason. There are  $2P_+$  terms where  $(n, m)$  are chosen such that  $q_n q_m = q^2$ , and  $2P_-$  where  $q_n q_m = -q^2$ . Since we are considering the case where  $(i, j)$  and  $(n, m)$  share both index values, selecting  $n$  and  $m$  also determines  $i$  and  $j$ . An additional factor of 2 accounts for the possible swap of values between  $i$  and  $j$ .

Similarly, we can compute  $b(k)$ :

$$\begin{aligned} b(k) &= 8(P_+ - P_-)(N-2)q^2(2R)^{N-3} \\ &\times \int_{[-R,R]^3} \cos(|x_1 - x_2|k)|x_1 - x_3| dx_1 dx_2 dx_3 \\ &= 64(N-2)(P_+ - P_-)q^2(2R)^{N-3} \\ &\times \sin(kR) \left( \frac{kR \cos(kR) + (k^2 R^2 - 1) \sin(kR)}{k^4} \right). \quad (81) \end{aligned}$$

Here, the factor  $8(N-2)(P_+ - P_-)$  is explained in a similar way as in the calculation of  $a(k)$ . Specifically, since  $(n, m)$  and  $(i, j)$  share only one index, after selecting  $(n, m)$ , a factor of 2 is needed to account for the choice of the common index between  $(n, m)$  and  $(i, j)$ , while  $N-2$  counts the number of possibilities for the non shared index. An additional factor of 2 accounts for the possible permutations of  $(i, j)$ .

Finally,  $c(k)$  is given by:

$$\begin{aligned} c(k) &= (N-2)(N-3)2(P_+ - P_-)q^2(2R)^{N-4} \\ &\times \int_{[-R,R]^4} \cos(|x_1 - x_2|k)|x_3 - x_4| dx_1 dx_2 dx_3 dx_4 \\ &= \frac{64}{3}(N-2)(N-3)(P_+ - P_-)q^2(2R)^{N-4}R^3 \frac{\sin^2(kR)}{k^2}, \quad (82) \end{aligned}$$

where the factor  $(N-2)(N-3)2(P_+ - P_-)$  accounts for the number of possible combinations of indices  $(i, j)$  and  $(n, m)$ , with all indices being distinct.

Plugging in Eq. (76) the results just found, we obtain the following expression for  $C(k, \beta)$ :

$$\begin{aligned} C(k, \beta) &= N(N-1)(2R)^{(N-2)} \frac{4 \sin^2(kR)}{k^2} \\ &+ \frac{\beta}{2} [a(k) + b(k) + c(k)] + O(\beta^2). \quad (83) \end{aligned}$$

We now substitute into Eq. (71) the expressions for  $C(k, \beta)$  from Eq. (83) and for the inverse partition function from Eq. (75), both valid at linear order in  $\beta$ . After performing the product and discarding the quadratic terms in  $\beta$ , the resulting expression for the DFF is

$$\begin{aligned} \text{DFF}(k) &= \frac{1}{N^2} \left( N + \frac{1}{Z} C(k, \beta) \right) \\ &= \text{DFF}_{(\text{BPP})}(k) \\ &+ \frac{\beta}{N^2(2R)^N} \left[ \frac{a(k) + b(k) + c(k)}{2} \right. \\ &\left. - \frac{4}{3} N(N-1)(2R)^{(N-1)} q^2 (P_+ - P_-) \frac{\sin^2(kR)}{k^2} \right]. \quad (84) \end{aligned}$$

Equation (84) shows that when  $\beta = 0$ , we recover the BPP case,

$$\lim_{\beta \rightarrow 0} \text{DFF}(k) = \text{DFF}_{(\text{BPP})}(k), \quad (85)$$

while the last line of Eq. (84) gives the first order correction in  $\beta$  for the Coulomb gas.

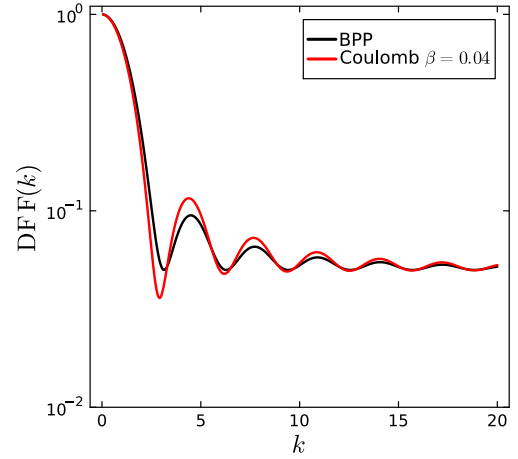


FIG. 5. Comparison of the DFF for a BPP, corresponding to  $\beta = 0$ , and a Coulomb gas with  $\beta = 0.04$  in 1D. The system consists of  $N = 20$  particles confined to the segment  $[-1, 1]$ , with each particle carrying a charge  $q = +1$ . The red curve represents the analytic expression for the Coulomb gas, given by Eq. (84), while the black curve corresponds to the analytic DFF of a BPP, as derived in Sec. IV. A logarithmic scale is used on the y-axis to highlight the differences between the two curves.

## B. Distance form factor of a Coulomb gas in higher dimensions

In this section, we extend the analytical result of the previous section using a numerical approach.

Since the charge labels the points, it is useful to decompose the DFF as

$$\begin{aligned} \text{DFF}(k) &= \frac{1}{N^2} \left\langle \sum_{i=1}^{N_+} \sum_{j=1}^{N_+} \cos(|\mathbf{r}_i - \mathbf{r}_j|k) + \sum_{i=1}^{N_-} \sum_{j=1}^{N_-} \cos(|\mathbf{r}_i - \mathbf{r}_j|k) \right. \\ &\left. + 2 \sum_{i=1}^{N_+} \sum_{j=1}^{N_-} \cos(|\mathbf{r}_i - \mathbf{r}_j|k) \right\rangle \\ &= \text{DFF}^{++}(k) + \text{DFF}^{--}(k) + \text{DFF}^{+-}(k), \quad (86) \end{aligned}$$

where the first two terms,  $\text{DFF}^{++}$  and  $\text{DFF}^{--}$ , account for points with the same charge, positive and negative respectively, whereas  $\text{DFF}^{+-}$  is computed by considering only the spacing between pairs of points with opposite charges. Figure (6) shows the DFF numerically computed for the Coulomb gas. Specifically, Panels (a), (c), and (e) display the component  $\text{DFF}^{+-}$  for a neutral Coulomb gas in different dimensions. Panels (b), (d), and (f) depict the DFF of a Coulomb gas where all the charges are positive, in different dimensions. As expected, when the value of the inverse temperature  $\beta$  tends to zero, the interaction vanishes, and we recover the BPP case. This can, in fact, be seen as the limiting case of a Coulomb gas at infinite temperature, where the thermal agitation is so intense that the interaction between points does not play a role.

As discussed in Sec. V, the DFF for a BPP in  $d > 1$  dimensions exhibits a feature analogous to the correlation hole observed in the SFF of a quantum system, which arises due to

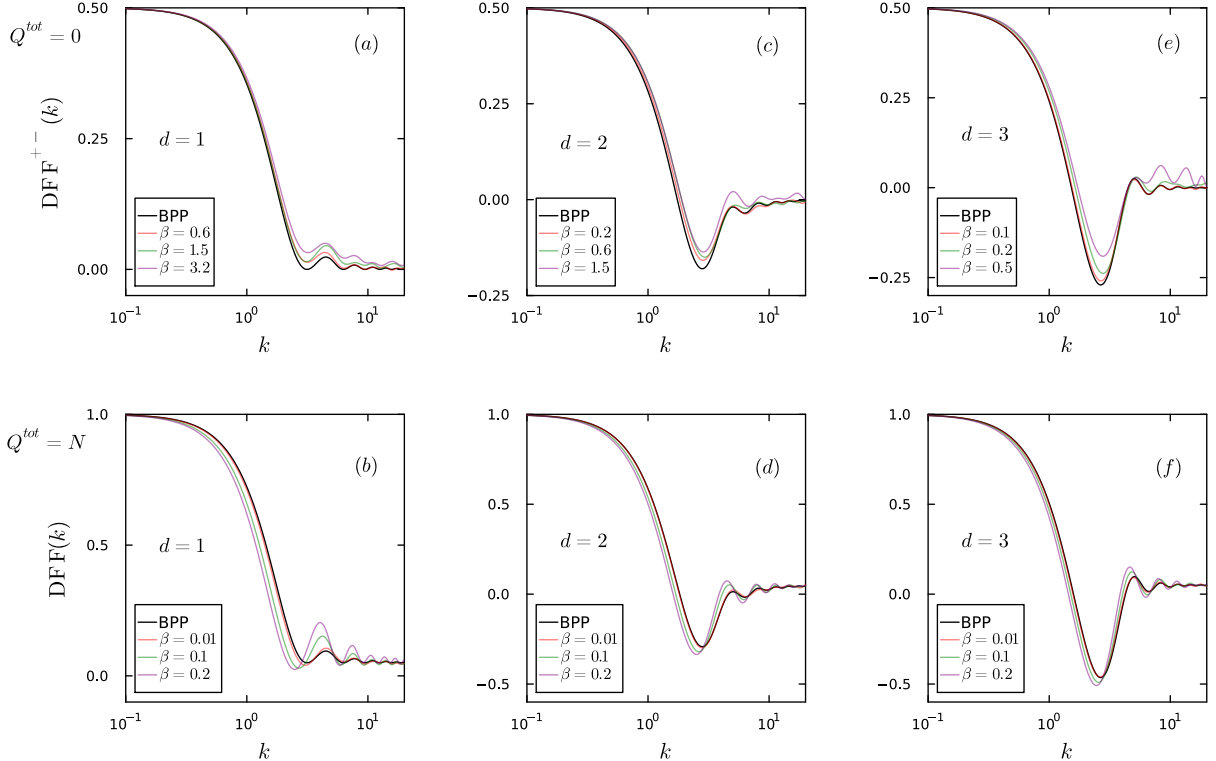


FIG. 6. Distance form factor of a system of  $N = 20$  points with Coulomb interaction for different values of the inverse temperature  $\beta$  in dimensions  $d = 1, 2, 3$ . The 1D system is represented by a segment of length  $2R = 2$ , while the 2D and 3D systems are represented by a disk and a sphere of unit radius, respectively. Panels (a), (c), and (e) correspond to a neutral Coulomb gas, depicting the component  $\text{DFF}^+$  of the distance form factor, which considers only the distances between opposite charges as per the decomposition in Eq. (86). Panels (b), (d), and (f) correspond to a gas of all positive charges, showing the corresponding full DFF. In each panel, the black line represents the analytic expression for DFF of the corresponding BPP, while the colored lines have been determined by a Monte Carlo simulation.

the presence of energy level repulsion. Similarly, this phenomenon in the DFF can be attributed to the behavior of the nearest neighbor spacing distribution  $P_d^{\text{NN}}(s)$ , given in Eq. (44), which vanishes for small  $s$ , giving rise to an apparent point repulsion.

In a Coulomb gas with  $\beta > 0$ , as demonstrated in Fig. (6), this effect can be either enhanced or diminished depending on the distribution of particle charge signs. Specifically, for a Coulomb gas with equal charges of the same sign, the leading correction in  $\beta$  leads to a faster decay from the unit value, reducing the value of the dip and enhancing the amplitude of the oscillations following it. This can be seen as a consequence of the repulsive interaction. On the other hand, in a neutral Coulomb gas, the component  $\text{DFF}^+$  exhibits a less pronounced dip. This results from the attraction between particles with opposite charges, which counteracts the point repulsion.

## VII. CONCLUSIONS AND DISCUSSION

In this work, we have introduced the distance form factor for the characterization of spatial point patterns and detailed

the analysis for random patterns. We have established two fundamental results. First, the DFF is related to the even Fourier transform of the probability distribution for the distance between any pair of points, which is familiar from the ball line picking problem in stochastic geometry [1, 54]. Second, we have established the relation between the DFF and the set of  $k$ -order spacing distributions. We have focused on the explicit computation of the DFF for homogeneous Poisson point processes in arbitrary dimensions, for which we have provided explicit expressions in terms of well-known functions.

The line-picking problem has been studied and finds application in many other enclosed regions in  $\mathbb{R}^d$ , such as convex polytopes, suggesting further extensions of our work to such geometries [1, 54].

With an eye on applications on nonequilibrium statistical mechanics and condensed matter physics, our results for the DFF are directly applicable to the characterization of random spatial patterns of point-like topological defects such as vortices, generated via the Kibble-Zurek mechanism [16], for which the accuracy of the Poisson point process has been established [32, 33]. A natural extension of our work involves the inclusion of interactions that can be either contact (e.g.,

soft or hard-core interactions between particles of finite radius) or with finite range. For instance, vortices on a plane are known to interact as a 2D Coulomb gas, motivating the evaluation of the DFF in such a setting, which we have discussed using a numerical approach. Another extension motivated by the possibility of probing vortex spatial statistics in experiments with ultracold gases [25, 55] is the inclusion of an external potential, which can make the spatial patterns inhomogeneous, according to the Inhomogeneous Kibble-Zurek mechanism [55–58]. Beyond these applications, the DFF should prove useful in analyzing and characterizing point processes in general, including the case of regular and quasiperiodic patterns, as proposed in Sec. III.

Finally, we note that the DFF can be generalized as

$$\text{DFF}(k) = \left\langle \frac{1}{|X|^2} \sum_{x,y \in X} \cos[d(x,y)k] \right\rangle \quad (87)$$

to an arbitrary metric space  $(M, d)$  [59] with a distance  $d(x, y)$

between points  $x$  and  $y$  of a set  $X \subseteq M$  with finite cardinality  $|X| < \infty$ . Such generalization applies to other fields, such as information theory [60], making it possible to analyze, e.g., sets of strings using the Hamming distance. In the same vein, it could be applied in information geometry to characterize the distance distribution between a set of probability distributions [61] and in quantum information theory for exploring the distance distribution of quantum states (or even quantum operations) in a given set [62].

## ACKNOWLEDGMENTS

The authors are indebted to Pablo Martínez-Azcona, Ruth Shir, András Grabarits, and Seong-Ho Shin for insightful discussions and comments on the manuscript. This research was funded by the Luxembourg National Research Fund (FNR), grant reference 17132060.

---

[1] S. N. Chiu, D. Stoyan, W. S. Kendall, and J. Mecke, *Stochastic Geometry and Its Applications*, Wiley Series in Probability and Statistics (Wiley, 2013).

[2] S. Torquato, Hyperuniform states of matter, *Physics Reports* **745**, 1 (2018), hyperuniform States of Matter.

[3] T. Guhr, A. Müller-Groeling, and H. A. Weidenmüller, Random-matrix theories in quantum physics: common concepts, *Physics Reports* **299**, 189 (1998).

[4] F. Haake, *Quantum Signatures of Chaos* (Springer, Berlin, 2010).

[5] O. Bohigas, M. J. Giannoni, and C. Schmit, Characterization of chaotic quantum spectra and universality of level fluctuation laws, *Phys. Rev. Lett.* **52**, 1 (1984).

[6] L. Leviandier, M. Lombardi, R. Jost, and J. P. Pique, Fourier transform: A tool to measure statistical level properties in very complex spectra, *Phys. Rev. Lett.* **56**, 2449 (1986).

[7] J. Wilkie and P. Brumer, Time-dependent manifestations of quantum chaos, *Phys. Rev. Lett.* **67**, 1185 (1991).

[8] Y. Alhassid and N. Whelan, Onset of chaos and its signature in the spectral autocorrelation function, *Phys. Rev. Lett.* **70**, 572 (1993).

[9] J.-Z. Ma, Correlation hole of survival probability and level statistics, *Journal of the Physical Society of Japan* **64**, 4059 (1995).

[10] J. Sakhr and J. M. Nieminen, Wigner surmises and the two-dimensional homogeneous poisson point process, *Phys. Rev. E* **73**, 047202 (2006).

[11] N. Manton and P. Sutcliffe, *Topological Solitons*, Cambridge Monographs on Mathematical Physics (Cambridge University Press, 2004).

[12] T. W. B. Kibble, Topology of cosmic domains and strings, *J. of Phys. A: Math. Gen.* **9**, 1387 (1976).

[13] T. W. B. Kibble, Some implications of a cosmological phase transition, *Phys. Reports* **67**, 183 (1980).

[14] W. H. Zurek, Cosmological experiments in superfluid helium?, *Nature* **317**, 505 (1985).

[15] W. H. Zurek, Cosmological experiments in condensed matter systems, *Phys. Reports* **276**, 177 (1993).

[16] A. del Campo and W. H. Zurek, Universality of phase transition dynamics: Topological defects from symmetry breaking, *International Journal of Modern Physics A* **29**, 1430018 (2014).

[17] P. M. Chesler, A. M. García-García, and H. Liu, Defect formation beyond kibble-zurek mechanism and holography, *Phys. Rev. X* **5**, 021015 (2015).

[18] H.-B. Zeng, C.-Y. Xia, and A. del Campo, Universal breakdown of kibble-zurek scaling in fast quenches across a phase transition, *Phys. Rev. Lett.* **130**, 060402 (2023).

[19] C.-Y. Xia, H.-B. Zeng, A. Grabarits, and A. del Campo, Kibble-zurek mechanism and beyond: Lessons from a holographic superfluid disk (2024), arXiv:2406.09433 [cond-mat.stat-mech].

[20] T. Vachaspati, *Kinks and Domain Walls: An Introduction to Classical and Quantum Solitons* (Cambridge University Press, 2023).

[21] P. Laguna and W. H. Zurek, Density of kinks after a quench: When symmetry breaks, how big are the pieces?, *Phys. Rev. Lett.* **78**, 2519 (1997).

[22] A. del Campo, G. De Chiara, G. Morigi, M. B. Plenio, and A. Retzker, Structural defects in ion chains by quenching the external potential: The inhomogeneous kibble-zurek mechanism, *Phys. Rev. Lett.* **105**, 075701 (2010).

[23] F. J. Gómez-Ruiz, J. J. Mayo, and A. del Campo, Full counting statistics of topological defects after crossing a phase transition, *Phys. Rev. Lett.* **124**, 240602 (2020).

[24] F. Suzuki and W. H. Zurek, Topological defect formation in a phase transition with tunable order, *Phys. Rev. Lett.* **132**, 241601 (2024).

[25] C. N. Weiler, T. W. Neely, D. R. Scherer, A. S. Bradley, M. J. Davis, and B. P. Anderson, Spontaneous vortices in the formation of Bose-Einstein condensates, *Nature* **455**, 948 (2008).

[26] N. Navon, A. L. Gaunt, R. P. Smith, and Z. Hadzibabic, Critical dynamics of spontaneous symmetry breaking in a homogeneous bose gas, *Science* **347**, 167 (2015).

[27] J. Goo, Y. Lim, and Y. Shin, Defect saturation in a rapidly quenched bose gas, *Phys. Rev. Lett.* **127**, 115701 (2021).

[28] J. Goo, Y. Lee, Y. Lim, D. Bae, T. Rabga, and Y. Shin, Universal early coarsening of quenched bose gases, *Phys. Rev. Lett.* **128**, 135701 (2022).

[29] A. del Campo, F. J. Gómez-Ruiz, Z.-H. Li, C.-Y. Xia, H.-B. Zeng, and H.-Q. Zhang, Universal statistics of vortices in a newborn holographic superconductor: beyond the kibble-zurek mechanism, *Journal of High Energy Physics* **2021**, 61 (2021).

[30] B. Ko, J. W. Park, and Y. Shin, Kibble–zurek universality in a strongly interacting fermi superfluid, *Nature Physics* **15**, 1227 (2019).

[31] K. Lee, S. Kim, T. Kim, and Y. il Shin, Observation of universal kibble-zurek scaling in an atomic fermi superfluid (2023), arXiv:2310.05437 [cond-mat.quant-gas].

[32] A. del Campo, F. J. Gómez-Ruiz, and H.-Q. Zhang, Locality of spontaneous symmetry breaking and universal spacing distribution of topological defects formed across a phase transition, *Phys. Rev. B* **106**, L140101 (2022).

[33] M. Thudiyangal and A. del Campo, Universal vortex statistics and stochastic geometry of bose-einstein condensation, *Phys. Rev. Res.* **6**, 033152 (2024).

[34] M. Allen and D. Tildesley, *Computer Simulation of Liquids*, Oxford science publications (Oxford University Press, 2017).

[35] M. N. M. van Lieshout, *Theory of Spatial Statistics: A Concise Introduction* (Chapman and Hall/CRC, 2019).

[36] M. Mehta, *Random Matrices* (Academic Press, 1991).

[37] J. S. Cotler, G. Gur-Ari, M. Hanada, J. Polchinski, P. Saad, S. H. Shenker, D. Stanford, A. Streicher, and M. Tezuka, Black holes and random matrices, *Journal of High Energy Physics* **2017**, 118 (2017).

[38] A. del Campo, J. Molina-Vilaplana, and J. Sonner, Scrambling the spectral form factor: Unitarity constraints and exact results, *Phys. Rev. D* **95**, 126008 (2017).

[39] R. Shir, P. Martínez-Azcona, and A. Chenu, Full range spectral correlations and their spectral form factors in chaotic and integrable models (2023), arXiv:2311.09292 [quant-ph].

[40] R. Penrose, Pentaplexity a class of non-periodic tilings of the plane, *The Mathematical Intelligencer* **2**, 32 (1979).

[41] B. Grünbaum and G. Shephard, *Tilings and Patterns*, Dover Books on Mathematics Series (Dover Publications, Incorporated, 2013).

[42] M. Kendall and P. Moran, *Geometrical Probability*, Griffin's Statistical Monographs (Hafner Publishing Company, 1963).

[43] L. Santaló, *Integral Geometry and Geometric Probability*, Cambridge Mathematical Library (Beijing World Publishing Corporation (BJWPC), 2004).

[44] I. Gradshteyn, A. Jeffrey, I. Ryzhik, and I. Ryzhik, *Table of Integrals, Series, and Products* (Academic Press, 1996).

[45] DLMF, *NIST Digital Library of Mathematical Functions*, <https://dlmf.nist.gov/>, Release 1.2.2 of 2024-09-15, f. W. J. Olver, A. B. Olde Daalhuis, D. W. Lozier, B. I. Schnei-  
der, R. F. Boisvert, C. W. Clark, B. R. Miller, B. V. Saunders, H. S. Cohl, and M. A. McClain, eds.

[46] P. Forrester, *Log-Gases and Random Matrices (LMS-34)*, London Mathematical Society Monographs (Princeton University Press, 2010).

[47] T. J. I. Bromwich, *An Introduction to the Theory of Infinite Series* (Macmillan and Company, 1908).

[48] W. Feller, *An Introduction to Probability Theory and Its Applications, Volume 2*, Wiley Series in Probability and Statistics (Wiley, 1991) p. 514.

[49] S. Serfaty, Systems of points with coulomb interactions, *EMS Newsletter* **110**, 16 (2018).

[50] A. del Campo, Exact ground states of quantum many-body systems under confinement, *Phys. Rev. Res.* **2**, 043114 (2020).

[51] M. Beau, S. M. Pittman, G. E. Astrakharchik, and A. del Campo, Exactly solvable system of one-dimensional trapped bosons with short- and long-range interactions, *Phys. Rev. Lett.* **125**, 220602 (2020).

[52] P. Le Doussal, Ranked diffusion, delta bose gas, and burgers equation, *Phys. Rev. E* **105**, L012103 (2022).

[53] M. Kardar, *Statistical Physics of Particles* (Cambridge University Press, 2007).

[54] A. Mathai, *An Introduction to Geometrical Probability: Distributional Aspects with Applications*, Statistical distributions and models with applications (Taylor & Francis, 1999).

[55] M. Kim, T. Rabga, Y. Lee, J. Goo, D. Bae, and Y. Shin, Suppression of spontaneous defect formation in inhomogeneous bose gases, *Phys. Rev. A* **106**, L061301 (2022).

[56] W. H. Zurek, Causality in condensates: Gray solitons as relics of BEC formation, *Phys. Rev. Lett.* **102**, 105702 (2009).

[57] A. del Campo, A. Retzker, and M. B. Plenio, The inhomogeneous Kibble-Zurek mechanism: vortex nucleation during Bose-Einstein condensation, *New J. Phys.* **13**, 083022 (2011).

[58] A. del Campo, T. W. B. Kibble, and W. H. Zurek, Causality and non-equilibrium second-order phase transitions in inhomogeneous systems, *Journal of Physics: Condensed Matter* **25**, 404210 (2013).

[59] D. Burago, I. Burago, and S. Ivanov, *A Course in Metric Geometry*, Crm Proceedings & Lecture Notes (American Mathematical Society, 2001).

[60] T. Cover and J. Thomas, *Elements of Information Theory* (Wiley, 2012).

[61] S. Amari, *Information Geometry and Its Applications*, Applied Mathematical Sciences (Springer Japan, 2016).

[62] M. Hayashi, *Quantum Information: An Introduction* (Springer Berlin Heidelberg, 2006).